Dalton Transactions

Accepted Manuscript

ROYAL SOCIETY OF CHEMISTRY

rsc.li/dalton

View Article Online
DOI: 10.1039/C6DT04785H

Journal Name

ARTICLE

Co(III) Complexes of (1,3-Selen-2-yl)hydrazones and Their Sulphur Analogues: Comparative Structural, Electrochemical, Computational and Biological Activity Study†

Received 00th January 20xx,
Accepted 00th January 20xx

DOI: 10.1039/x0xx00000x

www.rsc.org/

Nenad R. Filipović[a], Hana Elshaflu[b], Sonja Grubišić[c], Ljiljana S. Jovanović[d], Marko Rodić[d], Irena Novaković[c], Aleksandar Marinković[e], Ivana S. Djordjević[c], Haidong Li[f], Nešo Šojić[f], Aleksandar Marinković[b], Tamara R. Todorović[e,*]

First Co(III) complexes with (1,3-selenazol-2-yl)hydrazones as an unexplored class of ligands were prepared and characterized by NMR spectroscopy and X-ray diffraction analysis. Novel ligands act as NNN tridentate chelators forming octahedral Co(III) complexes. The impact of structural changes on ligands' periphery as well as isosteric replacement of sulphur with selenium on electrochemical, and electronic absorption features of complexes are explored. To support the experimental data, density functional theory (DFT) calculations were also conducted. Theoretical NMR chemical shifts, the relative energies and natural bond orbital (NBO) analysis are calculated within the DFT approach, while the singlet excited state energies and HOMO-LUMO energy gap were calculated with time-dependent density functional theory (TD-DFT). The electrophilic f^- and nucleophilic f^+ Fukui functions are well adapted to find the electrophile and nucleophile centres in the molecules. Both, (1,3-selenazol-2-yl)- and (1,3-thiazol-2-yl)hydrazone Co(III) complexes showed potent antimicrobial and antioxidant activity. Significant difference among them was a smaller cytotoxicity of selenium compounds.

Introduction

Antimicrobial resistance is a serious public health problem particularly in hospitals and other health care settings. During the last decade, due to an increase of pathogen resistance, the antimicrobial agents are losing their efficiency. The evolution of bacterial resistance can be attributed to the use and overuse of antibiotics and transmission of resistance within and between individuals. Therefore, there is an urgent need for development of new classes of antimicrobials that may not be as susceptible to bacterial resistance mechanisms as the current drugs.[1]

1,3-Thiazole is well recognized pharmacophore in medicinal chemistry and it is constituent of many drugs such as tiazofurin (antineoplastic agents), ritonavir (anti-HIV drug), ravuconazole (antifungal agent), nitazoxanide (antiparasitic agent), fanetizole (anti-inflammatory agent), and nizatidine (antiulcer agent).[2] The biological activity of their selenium analogues *i.e.* 1,3-selenazoles were studied to a much smaller extent. Up to now there are only three studies of anticancer and antimicrobial activity of 1,3-selenazoles.[3–5] Selenium, the essential trace element, is controversial regarding its biological activity. In 1930s it was marked as toxic, since it was regarded as a cause of plant-induced neuropathy of grazing horses and cattle. Twenty years later it was shown that Se prevented pathologies in vitamin E-deficient animals. The status of nutritional essentiality was extended to humans in the 1980s.[6] Selenium is both toxic to all organisms and essential to many bacteria and animal species.[7] As a heavier chalcogen element its chemistry is more similar to sulphur than to oxygen. On the other hand, there are some important differences between two chalcogens, especially in redox chemistry. Namely, selenium has ability to become rapidly oxidized and then to be rapidly reduced, which has been referred to as the "selenium paradox." Also, almost all chemical reactions involving selenium are faster in comparison to the same reactions with sulphur. The later was confirmed by the fact that replacement of Se with S resulted in mutant enzymes with greatly impaired

[a] Department of Chemistry and Biochemistry, Faculty of Agriculture, University of Belgrade, Nemanjina 6, Belgrade, Serbia.
[b] Faculty of Technology and Metallurgy, University of Belgrade, Karnegijeva 4, Belgrade, Serbia.
[c] Institute of Chemistry, Technology and Metallurgy, University of Belgrade, Njegoševa 12, Belgrade, Serbia.
[d] Department of Chemistry, Faculty of Sciences, University of Novi Sad, Trg Dositeja Obradovića 4, Novi Sad, Serbia.
[e] Faculty of Chemistry, University of Belgrade, Studentski trg 12–16, Belgrade, Serbia.
[f] University of Bordeaux, Bordeaux INP, ENSCBP, Institut des Sciences Moléculaires, CNRS UMR 5255, 16 Avenue Pey-Berland, 33607 Pessac, France.
† [*]Corresponding author. E-mail: tamarat@chem.bg.ac.rs.
Electronic Supplementary Information (ESI) available: includes full experimental procedures, electrochemical, computational and X-ray structural data, and NMR spectra. See DOI: 10.1039/x0xx00000x

View Article Online
DOI: 10.1039/C6DT04785H

catalytic activity, while replacement of S with Se in Cys-containing enzymes resulted in enhanced catalytic activity.[8]

The biological activity of selenium compounds has been studied to a much lesser extent in comparison to sulphur analogues. On the other hand, the comparative studies of isosteric selenosemicarbazones and thiosemicarbazones, precursors for synthesis of (1,3-selenazol-2-yl)hydrazones and (1,3-thiazol-2-yl)hydrazones, indicated the importance of the nature of chalcogen atom identity on biological activity.[9–19] The first comparative study of anticancer activity indicated that thiosemicarbazones are more potent antineoplastic agents and more active against malaria than selenosemicarbazones.[9,10] Latter studies demonstrated a pronounced improvement in selectivity toward neoplastic cells relative to normal ones by selenium compounds[11] and their better antiproliferative activity in comparison to sulphur analogues.[12,13] In terms of antimalarial activity, sulphur compounds were found to be more potent than selenium isosters,[14,15] while both classes of compounds showed equal potencies when they were tested as inhibitors of herpes simplex virus Type-1 specified ribonucleoside diphosphate reductase.[16] On the other hand, isosteric replacement of sulphur with selenium atom resulted in an improvement of the cruzipain inhibitory[17] and antimicrobial activity.[18,19]

(1,3-Thiazol-2-yl)hydrazones are a class of thiazoles which can be prepared by Hantzsch's reaction of thiosemicarbazones and α-haloarylcarbonyl compounds. They showed antituberculotic, antiparasitic, antioxidant and anticancer activities and potent inhibitory activities against human monoamine oxidase B and histone acetyltransferase.[20] Few studies indicated promising antimicrobial activity of (1,3-thiazol-2-yl)hydrazones.[20–23] On the other hand, to the best of our knowledge there is no antimicrobial activity study of (1,3-selenazol-2-yl)hydrazones. One strategy for the improvement of biological activity of organic compounds is the synthesis of their metal complexes. Upon coordination to metal ions, the lipophilic and aromatic parts of organic ligands are oriented outwards from the complex molecules toward the solvents. Metal complexes may act as a vehicle for the activation of the ligands by increasing their ability to diffuse through the semipermeable membrane of cells.[24] The major advantage of metal-complexes over corresponding organic ligands is the ability to vary coordination number and geometry. Also, access to redox chemistry is a clear advantage of metal complexes, since they generally have biologically accessible redox potentials.[25] Upon coordination to metals such as cobalt, obtained complexes often show improved activity and fewer side effects.[26] Cobalt is an element of interest for complex preparation since it is essential trace element found in all animals, and less toxic to humans than non-essential metals like platinum.[27] Recent studies indicate that many of cobalt complexes showed better antimicrobial activities when compared to free ligands themselves.[28] 1,3-Thiazoles act as ligands due to their ability to coordinate various metal ions. Their coordination ability is attributed to the presence of sulphur and nitrogen atoms in the five membered thiazole ring, but coordination capacity can be enhanced by structural modification and introduction of a variety of substituents with suitable donor atoms.[29] In our previous work we obtained the first single crystal X-ray diffraction structure of one (thiazol-2-yl)hydrazone Co(III) complex.[20] Our results indicated bis NNN tridentate coordination mode of 2-(2-(pyridine-2-ylmethylene)hydrazinyl)-4-(4-tolyl)-1,3-thiazole to Co(III). After 24 h incubation period this complex revealed stronger cytotoxic activity compared to cisplatin on MCF-7 breast cancer cell line. Experiments on MCF-7 3-D cell model resulted in complete suppression of spheroid growth.[20]

In order to get data about biological potency of (1,3-selenazol-2-yl)hydrazones in this work we prepared several pyridine based ligands (Scheme 1) and tested their antioxidant, cytotoxic and antimicrobial activity. The first Co(III) complexes with this class of ligands were prepared in order to obtain more potent derivatives (Scheme 1). Finally the comparative structural, electrochemical and DFT studies with sulphur analogues was done to elucidate in more detail the impact of chalcogen atom nature on chemical as well as biological features of these two classes of compounds.

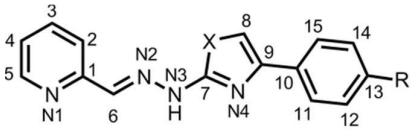

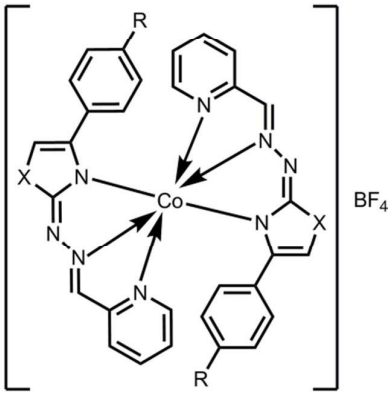

Ligand	R	X	Complex
HLS^1	H	S	**1-S**
HLS^2	OMe	S	**2-S**
HLS^3	Me	S	**3-S**
HLSe^1	H	Se	**1-Se**
HLSe^2	OMe	Se	**2-Se**
HLSe^3	Me	Se	**3-Se**

Scheme 1 Ligands and complexes included in the study.

DOI: 10.1039/C6DT04785H

Results and discussion

Synthesis and structural characterization

Preparation of **HLS$^{(1–3)}$** by reaction of 2-formylpyridine thiosemicarbazone (Hfptsc) with appropriate derivative of 2-bromoacetophenone in 2-propanol at room temperature was already described in the literature.[30] In this procedure $CaCO_3$ served as a base in order to prevent formation of HBr salts of desired thiazoles. In the case of **HLS^3** single crystals suitable for X-ray difraction analysis (XRD) were obtained by recrystallization from non-polar solvent mixture (toluene / hexane, 7 : 3, v/v).[30] XRD revealed that *Z* isomer of **HLS^3** was obtained. Our attempt to obtain all ligands from chalcogensemicarbazones and corresponding bromoacetophenones in EtOH as a solvent resulted in red precipitates for which, based on results of elemental analysis and molar conductivity measurements, general formula **HL(S/Se)$^{1–3}$ × HBr** can be established. Addition of water in DMF or EtOH solutions of **HL(S/Se)$^{1–3}$ × HBr** caused deprotonation and precipitation of neutral ligands in the form of yellow solids. Reaction of Hfptsc and 2-bromo-4'-methylacetophenone in EtOH / H_2O (1 : 1, v/v) mixture lead to formation of *E* isomer of **HLS^3** in the solid state as revealed by XRD.[20] *E* isomer also exists in solution, as confirmed by correlation signal of imine (HC=N–N) hydrogen and hydrazone (N–NH) hydrogen atoms in NOESY spectrum of **HLS^3**.[20] Here, the same solvent mixture was applied for preparation of **HL(S/Se)$^{1–3}$**. In NOESY spectrum of **HLSe^3** there is the same correlation signal which indicates the presence of *E*-**HLSe^3** isomer in DMSO-d_6 solution. Signals of imine hydrogen atom in ^{1}H NMR spectra of **HL(S/Se)$^{1–3}$** lie in the narrow region 12.38–12.54 ppm which is consistent with existence of *E* isomeric form of all lignads. Namely, formation of intamolecular hydrogen bond between N–NH hydrogen atom and pyridine nitrogen atom in *Z*-isomeric form of pyridine based hydrazones causes significant downfield shift (~ 2–3 ppm) of N–NH hydrogen atom signal.[31,32] The purity and composition of the ligands **HLSe$^{(1–3)}$** and **HLS$^{(1–3)}$** was confirmed by elemental analysis. Products were soluble in *N,N*-dimethylformamide (DMF) and dimethyl sulfoxide (DMSO), partially soluble in acetonitrile, chloroform, ethanol and methanol and insoluble in diethyl-ether and water. Structural characterization of the ligands was done by IR and NMR spectroscopy (Figures S1–S25, Electronic Supplementary Information).

In order to prepare Co(III) complexes of (1,3-selenazol-2-yl)hydrazone ligands the procedure we already used for preparation of Co(III) complex with **HLS^3** was employed.[20] Reactions of **HLSe$^{(1–3)}$** with $Co(BF_4)_2 \times 6H_2O$ in methanol afforded rotten-cherry coloured solutions. The same protocol was used for the preparation of new Co(III) complexes with **HLS$^{(1,2)}$**. After standing for three days emerald coloured single crystals were filtered off in all cases. Products were soluble in DMSO, DMF, MeOH, EtOH, acetonitrile and chloroform, and insoluble in diethyl-ether, ethyl-acetate and water. Magnetic measurements indicated that the complexes are diamagnetic in nature which allowed their structural characterization by NMR spectroscopy (Figures S26–S35, ESI). Diamagnetic behaviour of obtained complexes indicated that they contain Co(III) ions which are formed during air oxidation of Co(II) ions. Values of molar conductivity of all complexes in methanol suggest that they are 1 : 1 electrolytes. Elemental analysis showed that the complexes consist of Co^{3+} ion, two deprotonated ligand molecules and BF_4^- ion. Based on these results, the following general formula of the complexes can be postulated: $[Co(L_2)]BF_4$. In the case of complex with **HLSe^2**, obtained crystals were not of sufficient quality for XRD analysis. Better crystals of **2-Se** were obtained by diffusion of EtOAc into solution of **2-Se** in DMSO. The elemental analysis indicated the presence of one crystal water molecule in the obtained crystals of **2-Se**. For biological investigations, crystalohydrate was used. ^{1}H-NMR spectroscopy indicated an absence of N3 proton signal in spectra of all complexes which points to a coordination of corresponding ligands to Co(III) in their anionic form. In the IR spectra of all complexes strong absorption bands around 1050 cm^{-1} were found. These bands originate from BF_4^- ion and were not found in the IR spectra of free ligands.

A summary of the crystallographic data of the complexes are given in Table S1 (ESI). All the complexes consist of a complex cation $[CoL_2]^+$ and BF_4^- anions. Molecular structures of the complexes, with atom enumeration scheme of **1-S** as the representative, is given in Figure 1. Cations of the complexes have generally similar structures, closely related to the already published structure of **2-S.**[20] They are of the octahedral-type, with two meridionally placed ligands, and are therefore chiral. Seemingly, they have approximate C_2 symmetry where the two-fold axis is the bisector of N1A–Co1–N1B angle. Strictly speaking, only in the case of **1-S** the deviations from ideal C_2 point group symmetry are not significant, and C_2 symmetry of the cation is identified by *SYMMOL* algorithm,[33] with continuous symmetry measure of 1.41.[34,35] Additionally, the cation in **3-S** lies on a crystallographic two-fold axis, which imposes a perfect C_2 symmetry. In all other cases, no higher symmetry than C_1 was detected within default tolerance ranges.

In all five complexes the cobalt atoms are hexacoordinated. The geometry around cobalt atoms is octahedral, and the orthogonal nature of this coordination is clear from the angles between two chelate planes which are in the range 85.24(7)–89.28(5)° (Table 1; Figure S36, ESI). Ligands are coordinated in NNN tridentate way through the pyridine nitrogen, azomethine nitrogen, and nitrogen atom of the (selen/thi)azole ring. In that way two fused metallocycles are formed. Metal–ligand bond lengths are in the usual range (Table 1), and in all five complexes the bond between cobalt and azomethine nitrogen atom is the shortest. The observed trend that azomethine nitrogen atom makes shorter bond

View Article Online
DOI: 10.1039/C6DT04785H

than pyridine nitrogen atom is already noticed for the similar Schiff base ligands.[36–38]

Ligands are deprotonated at N3 position, which has as a consequence an electron delocalization through C7–N3 and C7–N4 bonds. These bonds are of similar lengths, despite the fact that C7–N3 bond is formally regarded as a double. In comparison to bond lengths in recently published structures of **HLS^3**,[20] **HLS^1**,[39] and *Z*-**HLS^3**,[30] bond lengths in coordinated ligands change so that C7–N3 is shortened, while C7–N4 is elongated.

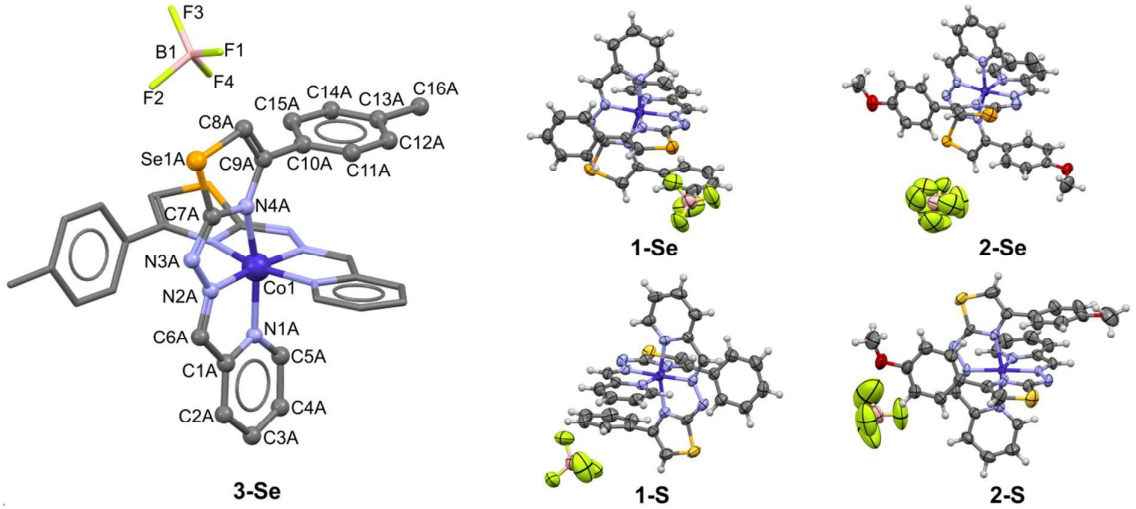

Fig. 1 Molecular structures of the complexes. Structure of **3-Se** is taken as the representative. Atom numbering scheme is given for one ligand. Atoms belonging to other ligand are enumerated in analogous way, with suffix *B*.

Table 1 Selected bond lengths (Å) for the complexes.

	1-S	**2-S**	**1-Se**	**2-Se**	**3-Se**
Co1–N1*A*	1.948(2)	1.948(5)	1.945(4)	1.965(4)	1.945(3)
Co1–N1*B*	1.946(2)		1.952(4)	1.940(4)	1.950(3)
Co1–N2*A*	1.888(2)	1.886(5)	1.887(4)	1.890(3)	1.890(2)
Co1–N2*B*	1.886(2)		1.879(3)	1.886(3)	1.885(2)
Co1–N4*A*	1.947(2)	1.948(6)	1.957(3)	1.949(4)	1.949(3)
Co1–N4*B*	1.945(2)		1.952(3)	1.964(4)	1.950(2)
C6*A*–N2*A*	1.293(4)	1.302(9)	1.286(5)	1.296(6)	1.286(4)
C6*B*–N2*B*	1.294(3)		1.294(5)	1.288(6)	1.301(4)
N2*A*–N3*A*	1.353(3)	1.359(8)	1.353(5)	1.341(6)	1.353(4)
N2*B*–N3*B*	1.350(3)		1.356(5)	1.343(5)	1.341(3)
C7*A*–N3*A*	1.336(4)	1.320(9)	1.339(6)	1.327(6)	1.343(4)
C7*B*–N3*B*	1.333(4)		1.328(6)	1.323(6)	1.342(4)
C7*A*–N4*A*	1.348(3)	1.346(7)	1.342(5)	1.354(6)	1.341(4)
C7*B*–N4*B*	1.346(3)		1.351(5)	1.350(6)	1.341(4)
C7*A*–X1*A*	1.725(3)	1.707(6)	1.862(4)	1.864(5)	1.868(3)
C7*B*–X1*B*	1.725(3)		1.870(5)	1.864(5)	1.867(3)
C8*A*–X1*A*	1.728(3)	1.729(11)	1.867(5)	1.875(5)	1.870(4)
C8*B*–X1*B*	1.729(3)		1.872(5)	1.864(6)	1.871(3)
C8*A*–C9*A*	1.353(4)	1.326(11)	1.345(6)	1.336(7)	1.345(5)
C8*B*–C9*B*	1.356(4)		1.350(6)	1.348(7)	1.343(5)
C9*A*–N4*A*	1.389(4)	1.393(8)	1.388(5)	1.395(6)	1.396(4)
C9*B*–N4*B*	1.384(4)		1.394(6)	1.394(6)	1.401(4)

X = S for **1-S** and **2-S**; X = Se for **1-Se**, **2-Se**, **3-Se**

DOI: 10.1039/C6DT04785H

It is important to note that the search of the Cambridge Structural Database (CSD) showed that there are no hitherto structurally characterized selenazole hydrazones, and **1-Se**, **2-Se**, and **3-Se** are thus the first crystallographically characterized complexes of selenazole hydrazones. Also, these complexes belong to a very few structurally characterized complexes with ligands coordinated through a selenazole ring,[40–43] and are so far the first with cobalt(III) as the central atom.

The complexes show some difference regarding the ligand molecules conformations. Namely, (selen/thi)azole ring can deviate from the chelate plane, and magnitudes of the deviations [2.6(2)–15.0(2)°] are not always similar for two ligands (A and B) in the same complex cation. Also, notable feature is the twisting of the terminal (substituted) phenyl ring (Figure 2). The angles between mean planes through those rings take values in the range 61.01(16)–88.62(10)°. A search of the CSD for angles between thiazole and phenyl rings, bonded the same as in present ligands, revealed a wide distribution of values, bimodal in nature with peaks around 7 and 45°. Out of 500 hits, only 32 angles were found with values > 60° (Figure S37, ESI).

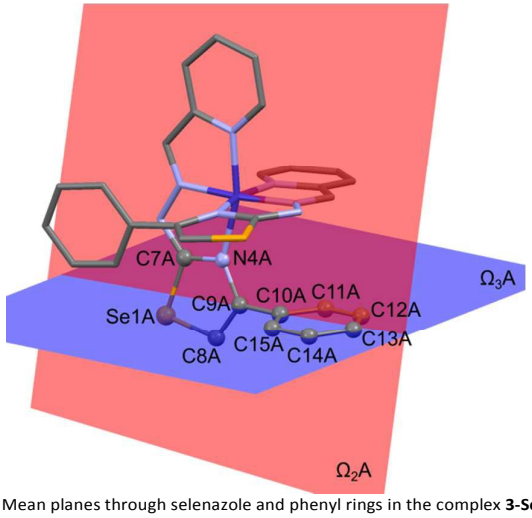

Fig. 2 Mean planes through selenazole and phenyl rings in the complex **3-Se**.

It is interesting to note that by doing so, terminal rings belonging to ligand A orient themselves more or less parallel with the chelate plane formed by ligand B, and *vice versa* (Figure S38, ESI), which is seen from corresponding angles that are in the range of 2.9(3)–12.83(19)°. It seems plausible that the observed conformations result in reduction of steric hindrance. Table 2 summarizes dihedral angles between mentioned planes for all complexes.

No classical hydrogen bonds are found in crystal structures of the complexes, as a consequence of the ligand deprotonation, and thus the lack of hydrogen bond donors. The pairs **1-S**–**1-Se**, and **3-S**–**3-Se**, crystallize in the same space groups with similar lattice parameters, and hence can be regarded as isostructural. Complexes **2-S**, **3-S**, and **2-Se** crystallize in non-centrosymmetric space groups, which means that spontaneous resolution of enantiomers occurs during crystallization. However, the crystal of **2-S** studied was twinned by merohedry, and its structure was refined as composed of four twin domains. The refined mass proportions of the domains indicate that specimen under study contained both enantiomers of the complex in approximately equal amounts.

The absorption spectra of selenazoles **HLSe**$^{(1–3)}$ and their sulphur analogues are given in Figure 3A, while their electronic absorption properties are summarized in Table 3. The longest wavelength of **HLSe**^{1} was observed at 366 nm, and bathochromic shift (of 4 and 8 nm respectively) was observed upon addition of methyl or methoxy group to the benzene ring. The longest wavelengths of sulphur analogues were observed at about 15 nm smaller values. These results implied both C13-subtituents and the nature of chalcogen atom strongly influenced the absorption spectra. Also, hypsochromic shifts of the absorption onset (λ_{onset}) of about 20 nm were observed in the case of thiazoles in comparison to their selenium analogues.

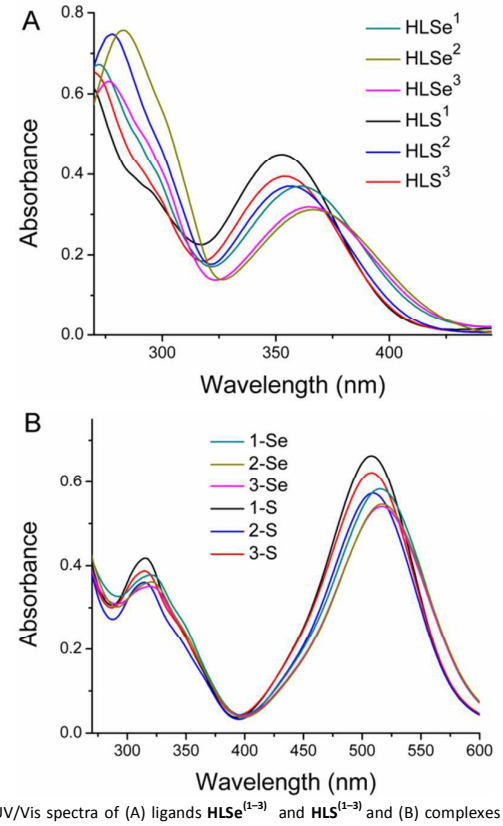

Fig. 3 UV/Vis spectra of (A) ligands **HLSe**$^{(1–3)}$ and **HLS**$^{(1–3)}$ and (B) complexes **(1–3)-Se** and **(1–3)-S**.

View Article Online
DOI: 10.1039/C6DT04785H

Table 2 Selected dihedral angles (°) for complexes.

	1-S	2-S	1-Se	2-Se	3-Se
$\angle(\Omega_1A\ \Omega_1B)$	89.28(5)	85.26(13)	89.33(8)	85.24(7)	88.28(7)
$\angle(\Omega_1A\ \Omega_2A)$	6.72(16)	5.7(5)	5.5(2)	2.6(2)	10.1(2)
$\angle(\Omega_1B\ \Omega_2B)$	5.16(14)	–	6.6(3)	15.0(2)	10.40(18)
$\angle(\Omega_2A\ \Omega_3A)$	88.62(10)	86.5(3)	81.99(14)	84.70(14)	78.75(10)
$\angle(\Omega_2B\ \Omega_3B)$	82.86(9)	–	87.62(14)	61.01(16)	73.43(11)
$\angle(\Omega_1A\ \Omega_3B)$	4.45(18)	10.5(4)	10.60(19)	10.7(2)	12.83(19)
$\angle(\Omega_1B\ \Omega_3A)$	9.90(13)	–	4.7(3)	2.9(3)	3.18(19)

Ω_1A and Ω_1B are chelate planes A and B defined as mean planes through atomsCo1 N1A N2A N4A, and Co1 N1B N2B N4B, respectively.
Ω_2A and Ω_2B are (selen/thi)azole planes A and B defined mean planes through atomsN4A C7A S1A/Se1A C8A C9A, and N4B C7B S1B/Se1B C8B C9B, respectively.
Ω_3A and Ω_3B are planes through terminal phenyl rings A and B defined mean planes through atoms C10A > C15A, and C10B>C15B, respectively.

Table 3 Electronic absorption properties and HOMO–LUMO energy gaps of **HLSe**[1–3] and **HLS**[1–3].

Ligand	λ_{abs}/nm	[calcd.] λ_{max}/nm	λ_{onset}/nm[a] (DMF)	HOMO-LUMO Band gap [eV]	
		π-π*		onset[b]	TD-DFT[c]
HLSe[1]	272, 366	243, 288, 379	421	3.26	3.28
HLSe[2]	283, 374	254, 295, 396	433	3.12	3.14
HLSe[3]	277, 370	246, 291, 383	425	3.22	3.24
HLS[1]	265, 352	240, 285, 371	402	3.33	3.35
HLS[2]	278, 358	252, 291, 388	411	3.19	3.20
HLS[3]	268, 355	244, 288, 376	405	3.29	3.30

[a] λ_{onset} are taken as the intersection of spectrum baseline and a tangent line to edge of the absorption band.
[b] HOMO–LUMO energy gaps calculated from λ_{onset}. [c] Calculated from λ_{max}, obtain from TD-DFT/B3LYP in DMF solvent, by using equation $E_{gap} = 1242/\lambda_{max}^{calc}$

Table 4 Electronic absorption properties and DFT calculation and assignment of λ_{max} (in nm) in DMF for **(1–3)-S** and **(1–3)-Se**.

Comp.	λ_{abs}/nm	[calcd.] λ_{max}/nm		HOMO–LUMO Band gap [eV]	
		$^1T_{2g} \leftarrow {}^1A_{1g}$ + LMCT	$^1T_{1g} \leftarrow {}^1A_{1g}$	λ_{max}[a]	TD-DFT[b]
1-Se	320, 516	363	507	2.41	2.45
2-Se	320, 517	364	513	2.40	2.47
3-Se	320, 516	363	503	2.41	2.42
1-S	315, 508	359	495	2.44	2.51
2-S	315, 509	360	504	2.44	2.46
3-S	315, 509	360	496	2.44	2.50

[a] Calculated from λ_{max}, obtained from TD-DFT/B3LYP/6-31G(d) in DMF solvent, by using Eq1: $E_{gap} = 1242/\lambda_{max}^{calc}$.
[b] Calculated from TD-DFT/B3LYP in DMF solvent as $E_{gap} = E_{HOMO} - E_{LUMO}$

The electronic absorption spectra of Co(III) complexes are given in Figure 3B. Two absorptions at almost the same wavelengths were found for **(1–3)-Se** (320 and 516 nm), while in the case of their sulphur analogues, a small bathochromic shift (of 5 and 7 nm, respectively) was noticed (Table 4). Selenium atom has the more spatially extended *p*- and *d*-orbitals, compared to those of sulphur atom, which leads to more effective delocalized electrons in conjugated systems of the selenazoles analogs and therefore the λ_{max} value of selenoazole ligands and complexes are shifted to a longer wavelength.

Voltammetric and spectoelectrochemical studies

All the ligands and the complexes were voltammetrically studied in DMF using tetrabutylammonium perchlorate (TBAP) as supporting electrolyte. In the available potential range (–2.1 V to +1.5 V) the ligands show mainly one reduction and one oxidation well-defined process (Figure 4A).

The reduction processes for the ligand molecules are located in a 1-e^- wave at potentials from around –1.6 V. Electrochemical characteristics of the peaks are: $\Delta E_p/\Delta \log v \sim$ –40 mV/dec, $I_p/cv^{1/2} \sim$ const, $E_p^a - E_p^c \sim 110$ mV (at v = 0.1 V/s). The gain in I_p^R on repetitive cycling in the amplitude more

DOI: 10.1039/C6DT04785H

negative than 0 V is about 80–100% of the starting one, depending on the sweep rate. This is an indication of a chemical instability of the reduced species resulting in a small ill-shaped oxidation peak near 0 V. The nature of this reaction with adsorptive complications was not studied in more detail. This corresponds to an irreversible process (Figure 4A).

The voltammogram shows an irreversible oxidation wave at potentials ~ +0.7 V. The anodic process is complicated by a slow chemical reaction giving rise to a species oxidized at more positive potentials (for ~ +0.07 V). After these oxidation processes several small peaks appear at the subsequent cathodic sweep pointing to a decomposition of the oxidized species of the products which were not identified.

The potentials of characteristic peaks of all ligands are given in Table S2 (ESI). Similar values of the potential and current functions are due to small differences in the electroactive centres. The one-electron reduction is located at C=N hydrazone group as it is common for these types of compounds.[44] Two-electron oxidations most probably occur at chalcogen and C8 atoms. Fukui function calculations reveal that these centres have the greatest f^- values, which points to their ability of electron donation (*vide infra*).

All six complexes in DMF show reduction and oxidation processes according to the same pattern, differing slightly in the main current and potential characteristics due to coordination effects.

The typical voltammograms of the complexes recorded in negative direction (reduction processes) are given in Figure 4B. Two pairs of apparently reversible one-electron peaks (at about –0.27 V and –1.27 V) are shown, accompanied by a large oxidation peak at ~ +1.2 V. The potentials of the reduction processes are given in Table 5. The voltammetric characteristics of both processes with $\Delta E_p(_{O/R})$ from 62 mV (at 0.01 V/s) to ~ 100 mV (at 2 V/s) give the values of heterogeneous rate constants[45] of about $(1–2)\cdot10^{-4}$ m/s (Table S3, ESI) which lie at the lower limit of rate constants for reversible systems.[46] In calculations the diffusion coefficient D value of $3.1\cdot10^{-10}$ m^2/s was used for all the complexes. This value was previously determined for similar bis(ligand) octahedral Fe(III) complexes with ligands based on thiosemicarbazones under the same experimental conditions[47] and was used as a substitute in a lack of true D values for the present complexes.

The expected number of reduction processes in the case of Co(III) octahedral complexes with pyridine-based Schiff base ligands containing C=N hydrazono group is four (three one-electron reductions at Co(III) central atom, i.e. Co(III)→Co(0) and one one-electron reduction of C=N group). However, only two reductions (Co(III)→Co(II) and Co(II)→Co(I)) are observed down to –2.0 V which correspond to processes at the central metal atom, as confirmed by spectroelectrochemical experiments (see below). The other reductions are obscured in a huge multi-electron peak arising around the negative potential limit in DMF. Here, similarly to previously reported Fe(III) complexes with heterocyclic chalcogensemicarbazones,[48] the potentials of reduction processes at coordinated ligands are 400–500 mV more negative comparing to the free ones, due to redistribution of negative charge.

However, oxidation process is much more complicated and its consequences on the behaviour of the complexes can be seen in consecutive scans. First, current function of the oxidation peak changes from 5-6 times greater than a 1-e^- reduction process at low sweep rates to only 4 times greater at high sweep rates. This could mean that with lowering the sweep rate the process changes from two-step 1-e^- release at each ligand particle to one-step 2-e^- oxidation process at each of the ligands at a close potential. The consequences of these changes can be followed in a subsequent negative sweep using variation of the sweep rate and the amplitude (Figure 4B-F). At sweep rates higher than 0.02 V/s a new species reducible at potentials ~ 150 mV more positive than the peak I_R and II_R replaces partially or completely the starting one (Figure 4B second sweep, 4C-E). At a closer insight into the consequences of the oxidation process, a new peak at ~ 0.7 V appears belonging to oxidation of the free ligand (Figure 4C) which was released after reduction of this instable complex. In addition, variations of the sweep rates in full potential amplitude reveal the presence of complex homogenous equilibrium coupled to redox processes which is also more pronounced with increasing the sweep rates (Figure 4F). Thus, it can be assumed that oxidation may proceed apparently uncomplicated if enough time to allow necessary reorganization of the oxidized complex is provided (Figure 4E,F). In other words, oxidation might cause temporary disturbances in the molecule which need time to re-establish the previous molecular symmetry. Thus, at low sweep rates this adjustment proceeds in parallel with electron release so the molecule seems to be stable at the end of the oxidation process.

The *in situ* spectroelectrochemistry of **3-S** was performed in solution to evaluate the spectral changes between its initial and reduced states. This is of importance for assigning in more details the electrochemical processes.[49,50] The Co(III) complex **3-S** was dissolved in a DMF solution containing 0.1 M $TBAPF_6$ and the absorption spectroelectrochemical studies were done using a Pt mesh working electrode. Previously, we recorded the cyclic voltammograms of **3-S** on a Pt electrode (data not shown) and the voltammetric behaviour (i.e. potential, reversibility, current) was identical with GC electrode material. UV-Vis spectroelectrochemical measurements were performed by using a thin-layer electrochemical cell of 1-mm optical path. As already mentioned, **3-S** presents two one-electron reversible reduction waves at −0.26 V and −1.28 V (Table 5). Therefore we studied the spectral changes for both reduced forms by applying potentials slightly more cathodic than the peak potential values (i.e. −0.5 and −1.5 V, respectively).

View Article Online
DOI: 10.1039/C6DT04785H

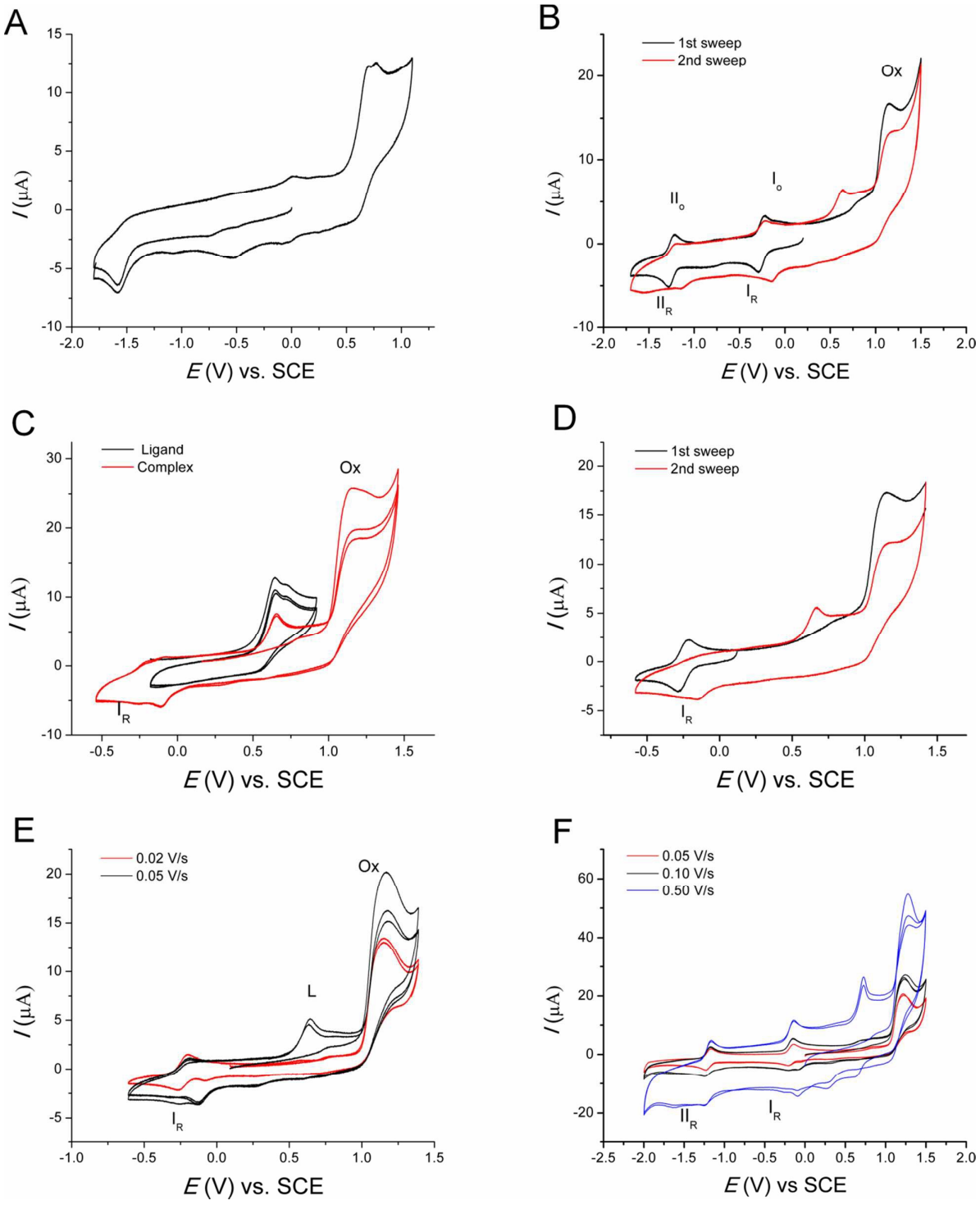

Fig. 4 Representative cyclic voltammograms of selected substances in DMF + 0.1 M TBAP, GC electrode: (A) **HLSe**^{3} (c = 0.44 mM, v = 0.1 V/s). (B) **3-Se** (c= 0.22 mM, v = 0.1 V/s). Full amplitude and cathodic sweep direction. (C) **2-Se** (c = 0.42 mM) and **HLSe**^{2} (c = 0.46 mM), v = 0.1 V/s. Narrow amplitude, anodic direction. (D) **3-Se** (c = 0.22 mM, v = 0.1 V/s). Narrow amplitude and cathodic sweep direction. (E) **2-S** (c = 0.40 mM) v = 0.02 and 0.05 V/s. Narrow amplitude and anodic direction. (F) **2-S** (c = 0.40 mM, v = 0.05, 0.1 and 0.5 V/s). Full amplitude and anodic direction.

View Article Online
DOI: 10.1039/C6DT04785H

Table 5 Voltammetric characteristics of the complexes.*

Complex	$E_p^R(I)^a$	$E_p^O(I)$	$I_R^I/cv^{1/2b}$	$E_p^R(II)$	$E_p^O(II)$	$I_R^{II}/cv^{1/2}$	E_p^{Ox}	$I_{Ox}/cv^{1/2}$
1-Se	–0.27	–0.20	45.0	–1.27	–1.20	43.1	1.16	225
2-Se	–0.30	–0.23	33.0	–1.28	–1.20	33.1	1.14	164
3-Se	–0.28	–0.21	36.1	–1.27	–1.20	33.0	1.16	202
1-S	–0.24	–0.17	37.4	–1.28	–1.21	38.9	1.20	214
2-S	–0.26	–0.20	37.3	–1.29	–1.22	36.0	1.19	189
3-S	–0.26	–0.18	37.5	–1.28	–1.21	37.1	1.20	196

*At v = 0.10 V/s. [a] In V. [b] In μA/mM(V/s)$^{1/2}$.

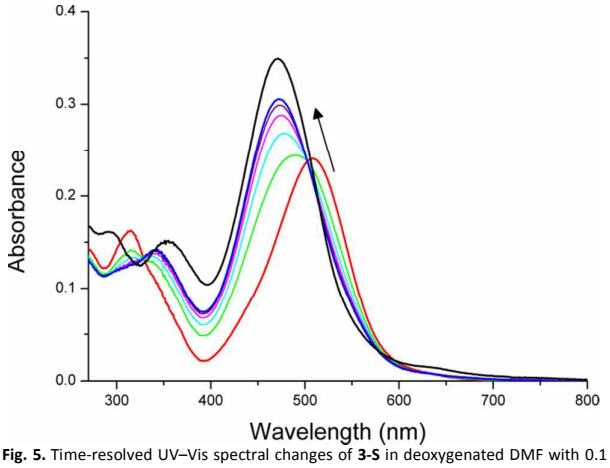

Fig. 5. Time-resolved UV–Vis spectral changes of **3-S** in deoxygenated DMF with 0.1 M $TBAPF_6$ before (red curve) and after applying the first reduction potential −0.5 V. The arrow indicates the evolution. Blue curve corresponds to the spectrum of the first reduced form. Black curve is the spectrum recorded at the equilibrium after applying −1.5 V.

Upon the first reduction potential −0.5 V, the evolution of the UV-Vis spectra with time were collected and depicted in Figure 5. Interestingly, the monitoring of the absorption revealed a fast and nice modification of the electronic transitions when the first reduced state is reached. As shown in Figure 5, the main band peaking initially at 509 nm is affected upon the first cathodic reaction. Indeed, it is blue-shifted and increased progressively. The small band at 315 nm tends to vanish. Applying a more cathodic potential (i.e. −1.5 V) corresponding to the second reduction process increases even more the main band which peaks now at 470 nm. In addition, two small bands appeared between 270 and 400 nm after adding this second electron to the complex. After approaching the equilibrium in both cases (E = −0.5 V and −1.5V), an open circuit potential (E = 0.1 V) was applied to the system. The absorbance recovered with time until the spectral signatures of the complex were as same as the initial state. It confirms the reversibility observed by cyclic voltammetry for the reduction processes and it shows that the reduced species are stable during the timescale of spectroelectrochemical experiments. Whatever, the main band at 509 nm of the initial **3-S** complex was attributed to the ligand to metal charge transfer transition (LMCT) as detailed in Table 4. The two reduction processes generate the Co(II) and then Co(I) from the initial Co(III) ion so it makes the LMCT transition more difficult. It explains that this main band was observed at a lower wavelength (i.e. higher energy) compared with that of the initial complex.[49–51] The spectroelectrochemical experiments demonstrate that the cathodic reactions correspond to two successive 1-e^- reduction of the central Co(III) atom of the complex.

DFT calculations

The selected DFT/B3LYP/6-31G(d) method for neutral *E*- and *Z*-isomeric form of ligands has been chosen from the consideration of several approaches already applied to similar molecular structures elsewhere.[52,53] Optimized structures of the ligands are shown in Figure S39 (ESI), and the relevant structural parameters in Table S4 (ESI). Structural data of all optimized molecules correspond reasonably well to the XRD data of available crystal structures. In addition, an evaluation of reliability of theoretical calculations also includes prediction of the planarity of the investigated molecules. There is a very good agreement between experimental and calculated dihedral angles. By comparing N_3–H bond lengths of **HLS**[1] ligand, it can be observed that these bonds are longer in the *Z*-isomer (Table S4, ESI). The present theoretical method successfully reproduces experimentally observed formation of intramolecular H-bond between N1 of pyridine ring and the proton attached to N3 of hydrazone group CH=N–NH–.[30] Calculated relative energy shows that *Z*-isomer is more stable than *E*-isomer (Table S5, ESI). This observation can be explained by the presence of stabilizing effect in *Z*-isomeric form due to a formation of intramolecular H-bond.[54]

In order to evaluate the basis set influence on the geometry of Co(III) complexes, for the **1-S** complex we have applied two DFT models, B3LYP and BVP86, as well as several basis sets of various complexity. There is a noticeable tendency for increasing bond length with increasing basis set size (Table S6, ESI). In fact, the smallest basis set for the metal ion gives the best agreement with the crystallographic data in the case of the Co–N bonds. Consistent with previous studies,[55] the BVP86/6-31g(d,p)/6-31g(d) method gives smallest differences

View Article Online
DOI: 10.1039/C6DT04785H

between experimental and calculated values of Co–N bond distances, especially for the Co–N4 bonds (Table S6, ESI). Optimized structures of complexes are shown in Figure S40 (ESI). Selected structural parameters for all Co(III) complexes are listed in Table S7 (ESI). Structural data of all optimized molecules correspond well to the data obtained from X-ray.

Chemical shifts for the complexes were calculated within GIAO approach at DFT/PCM(DMSO)/B3LYP level of theory. Results of theoretically predicted isotropic chemical shifts with respect to tetramethylsilane (TMS) are listed in Table S8 (ESI) and reveal a good match to the experimental spectroscopic data. Substitutions of Y = H with Y = CH_3, or OCH_3 have an expected influence on proton chemical shifts in *ortho*-position to the substituent Y of the benzene ring (upfield shifts).

Linear regression analysis was applied to estimate the correlation between experimental and calculated values of the chemical shifts. The analysis included experimental and calculated values of all C-sp^2 atoms, as well as, all chemical shifts of the protons attached to C-sp^2 atoms. The resulting linear regression lines were $\delta_{calc.} = 0.43 + 0.98\delta_{exp.}$ (R = 0.98, the correlation coefficient at confidence level of 95.0%) and $\delta_{calc.} = 0.24 + 0.97\delta_{exp.}$ (R = 0.79, the correlation coefficient at confidence level of 95.0%) for ^{13}C and ^{1}H NMR chemical shifts, respectively. Although, both values of R show a significant correlation between experimental and calculated chemical shifts, additional *two-sided t* test has been applied,[56] which confirmed the obtained liner regression results. The linearly scaled calculated values are listed in Table S8 (ESI).

The evaluation of absorption spectra and transition energies was carried out within the time dependent density functional theory (TD-DFT) approach, using B3LYP functional and DMF as solvent. In order to compare the spectral characteristics of Co(III) complexes with 1,3-selenazoles and 1,3-thiazoles as ligands, the absorption spectra, HOMO and LUMO energy levels, and the energies of HOMO-LUMO transitions (E_{gap}) were calculated.

The calculated electronic spectra of free ligands show shoulder bands in the range 240–255 nm (41596–39317 cm^{-1}) and two bands in the range 285–295 nm (35120–33937 cm^{-1}) and 370–395 nm (26929–31939 cm^{-1}). Calculated electronic transitions (λ), oscillator strengths (*f*) and major MO contributors to the transitions of **HLS$^{(1–3)}$** and **HLSe$^{(1–3)}$** ligands are listed in Table S9 (ESI). The shoulder band may be assigned to the π-π* transition of the thiazole and selenazole rings.[57] The absorption peak in the range 285–295 nm is due to π-π* transition of phenyl and pyridine rings.[58,59] The absorption maxima in the range 370–395 nm correspond to the π-π* transition of the azomethine moiety[60] with a contribution of the intraligands π-π* transitions.[57–59] The calculated wavelengths originating from π-π* transitions of phenyl, and pyridine rings, as well as those from azomethine moiety, are in good agreement with experimental values (Table 3). E_{gap} values of the ligands calculated from λ_{max} by TD-DFT method, are also in good agreement with values obtained by UV-Vis spectroscopy (Table 3). Due to higher degree of aromaticity of selenazole in comparison to thiazole, it can be expected for Se-heterocycles to be more stable and less reactive.[61] Calculated relative energies of the ligands indeed show that selenazoles are more stable than their thiazole analogs (Table S5, ESI). Also, all the selenazoles have the smaller values of E_{gap} than their sulphur analogs (Table 3), which indicates the lower reactivity of 1,3-selenazoles and explains the bathochromic shifts of absorption maxima.

Graphic representations of calculated HOMO, LUMO and HOMO-LUMO transitions for ligands are shown in Figure S41 (ESI). The HOMOs of all ligands are delocalized mainly at the azomethine group, heterocyclic ring and phenyl group, whereas the LUMOs are delocalized on the pyridine ring, azomethine group and the heterocyclic ring. The presence of electron releasing substituent (methyl- or methoxy-) of the thioazole and selenazole attached phenyl ring, destabilizes HOMO and LUMO orbitals and decreases the energy gap (Figure S41, ESI). Energetically the most favourable π-π* absorptions (370–395 nm) occur from HOMO→LUMO transitions (Table S9, ESI).

Since the intraligand π-π*, ligand to metal charge transfer (LMCT), or spin-forbidden transitions may cause broadening or masking of d-d bands[57–59] or even their disappearance[62] in the experimental absorption spectra of complexes, additional information could be obtained using the results of TD-DFT calculations, as discussed below.

The ground state of Co(III) ion in octahedral low-spin complexes is ^1A_g arising from $(t_{2g})^6$ electronic configuration. The one-electron excited states $^1T_{1g}$, $^3T_{1g}$, $^1T_{2g}$ and $^3T_{2g}$ derive from $(t_{2g})^5$ $(e_g)^1$ electronic configuration, of which both spin-triplet states lying at lower energy than the singlets.[63] Therefore, UV-VIS spectra of Co(III) ion in strong ligand field of O_h symmetry have the following assignments of d–d transitions: two spin allowed ν_1: $^1T_{1g} \leftarrow {}^1A_{1g}$; ν_2: $^1T_{2g} \leftarrow {}^1A_{1g}$ and two spin forbidden ν_3: $^3T_{1g} \leftarrow {}^1A_{1g}$; ν_4: $^3T_{2g} \leftarrow {}^1A_{1g}$.[64] Calculated electronic spectra of approximate octahedral **(1–3)-Se** and **(1–3)-S** complexes in DMF show two principal spin allowed bands. The first ones, relatively sharp around 20 000 cm^{-1} (500 nm), were assigned to $^1T_{1g} \leftarrow {}^1A_{1g}$ transition, while the second ones, broad around 30 000 cm^{-1} (360 nm), were assigned to $^1T_{2g} \leftarrow {}^1A_{1g}$. The electronic spectral assignments of the complexes are given in Table 4. E_{gap} values of complexes obtained via TD-DFT calculated from λ_{max} are also in a good agreement with experimental data (Table 3).

Ligand to metal charge transfers can be divided in four classes: ν_1: π→t_{2g} (π*), ν_2: π→e_g (σ*), ν_3: σ →t_{2g} (π*) and ν_4: σ →e_g (σ*) in order of increasing energy. For d^6 complexes, only ν_2 (25000-45000 cm^{-1}) and ν_4 (above 45000 cm^{-1}) transitions are spin allowed. In the investigated complexes π→e_g (σ*) transition can be the reason for broadening of the d-d band around 30000 cm^{-1} (360 nm). The important contribution can be assigned to the intervening sigma bond, which can be formed by donation of the nitrogen lone pairs (azomethine group) to the empty *d* orbital of the metal ion.[57–59] Presence of intraligand π-π* transitions may also cause a broadening of the absorption bands. Calculated electronic transitions (λ), oscillator strengths (*f*) and major MO contributors to the transitions of **(1–3)-Se** and **(1–3)-S** complexes are listed in Table S10 (ESI).

View Article Online
DOI: 10.1039/C6DT04785H

Graphic representations of calculated HOMO, LUMO and HOMO-LUMO transitions for complexes are shown in Figure 6. The LUMO orbitals of all Co(III) complexes are delocalized mainly at the azomethine group, metal centre, and pyridine ring. The main contribution to the HOMO orbitals of all Co(III) complexes derives from the heterocyclic ring, azomethine group, and metal centre.

It is known that DFT exchange-correlation functionals overestimate the energy of HOMO orbital and underestimate the energy of LUMO orbital. The HOMO eigenvalues predicted by hybrid functionals are generally better than those predicted by nonhybrid functionals, and their accuracy depend on the included percentages of Hartree-Fock exchange.[65] DFT/B3LYP calculated energies of HOMO orbitals for Co(III) complexes are in good agreement with experimental data (Table 6).

Table 6 Electrochemical properties and energies of HOMO orbitals of **(1–3)-S** and **(1–3)-Se**.

Compound	$E^{1/2}$ox/[eV][a]	HOMO/eV	
		CV[b]	DFT[c]
1-Se	0.532	–5.33	–5.52
3-Se	0.513	–5.31	–5.47
2-Se	0.500	–5.30	–5.48
1-S	0.568	–5.37	–5.52
2-S	0.540	–5.34	–5.52
3-S	0.554	–5.35	–5.50

[a]V vs F_c/F_c + in DMF containing 0.1 M TBAP as supporting electrolyte at a scan rate of 100 mV/s. GC working electrode. [b]E_{HOMO} (eV) = −4.8 − (E_{onset} −$E_{1/2(Fc/Fc+)}$).[60] [c]E_{HOMO} (eV) calculated from TD-DFT/DMF calculations.

Fukui functions (*f*) provide information about atoms in a molecule that have increased tendency to either lose or accept an electron. This allows evaluating the nucleophilic and electrophilic behaviour of each atom in a molecule. The greatest values of Fukui functions calculated by NBO charges at DFT/DMF of investigated ligands are reported in Table S11 (ESI). The f^- measures reactivity with respect to electrophilic attack or the tendency of the molecule to donate electrons, while f^+ measures reactivity related to nucleophilic attack or the propensity of a molecule to accept electrons. The highest value of f^- for the ligands is at Se/S and C8 indicating the zone for transfer of electron, while the highest value of f^+ is associated with N2 and C6 showing the ability for a back donation through the N2=C6 zone of hydrazone group.

Antimicrobial activity

The antimicrobial activity of the (1,3-thiazol-2-yl)hydrazones and (1,3-selenazol-2-yl)hydrazones and its Co(III) complexes was examined against four Gram-negative bacteria *P. hauseri, P. aeruginosa, E. coli, S. enterica* and four Gram-positive bacteria: *S. aureus, C. sporogenes, B. subtilis* and *K. rhizophila* (Table 7). Antifungal activity of investigated compounds was examined against *A. brasiliensis, C. albicans* and *S. cerevisiae* (Table S12, ESI).

From the results of antimicrobial activity investigation the impact of chalcogen atom identity on activity of organic ligand can be clearly seen. Namely, none of the sulphur ligands did show any activity against bacteria, while the activity against fungi was never higher in comparison to their selenium isosters. In the case of selenium ligands **HLSe$^{(1–3)}$**, substitutions on benzene ring often resulted in increased activity of the corresponding ligand in comparison to **HLSe^1** on all bacterial and fungi strains. The similar effect was found for **HLS$^{(1–3)}$** on all investigated fungi strains.

Complex formation enhanced to a great extent the activity of organic ligands against bacterial strains investigated. The trend found for the ligands is also valid for the complexes: **1-Se** and **1-S** were less active corresponding complexes.

The most potent thiazole complex appears to be **3-S**, while in the case of selenazoles the most active complex was **2-Se**. Contrary to ligands, in the case of Co(III) complexes it was not possible to establish a strict correlation of impact of isosteric replacement on antibacterial activity. Only in the case of **2-S** and **2-Se** sulphur analogue was more active on all investigated bacterial strains. **3-Se** was more active than **3-S** on all bacterial strains except *E. coli* and *K. rhizophila*, while **1-S** showed better activities against *E. coli, S. eneterica, B. subtilis* and *K. rhizophila* and its selenium analogue was more active against *P. hauseri, P. aeruginosa, S. aureus* and *C. sporogenes*.

In almost all cases a complex formation resulted in more active chemical species regarding antifungal activity, with few exceptions. Complexation of **HLS^2** with Co(III) resulted in **2-S** which showed no activity against *A. brasiliensis* and reduced activity against two other fungi strains. Reduced activity was also noticed for **2-Se** on *S. cerevisiae*. Slightly reduced activity was observed for **3-Se** in comparison to its parent ligand. The most active complexes on fungi strains were **1-Se** and **1-S** (with no substituents on benzene ring). The activity of **1-Se** against *C. albicans* was almost the same as in the case of nystatin (Table S12, ESI).

Acute lethality study

Results of acute toxicity test on brine shrimp (*Artemia salina)* caused by applied treatments are presented in Table 8. While DMSO itself did not cause changes in viability of treated nauplii at any of five tested concentrations, treatment with $K_2Cr_2O_7$ induced high incidence of lethality. Nauplii revealed different level of sensitivity toward (1,3-thiazol-2-yl)hydrazones and (1,3-selenazol-2-yl)hydrazones. Namely, our results showed that selenium compounds exhibited significantly reduced toxicity in comparison to their isosters. The most toxic were ligands without substituents at benzene ring (**HLS^1** and **HLSe^1**), while the most toxic sulphur base complex was **1-S**. In the case of selenium based complexes **1-Se** and **3-Se** showed the same level of toxicity, while the most toxic was **2-Se**.

View Article Online
DOI: 10.1039/C6DT04785H

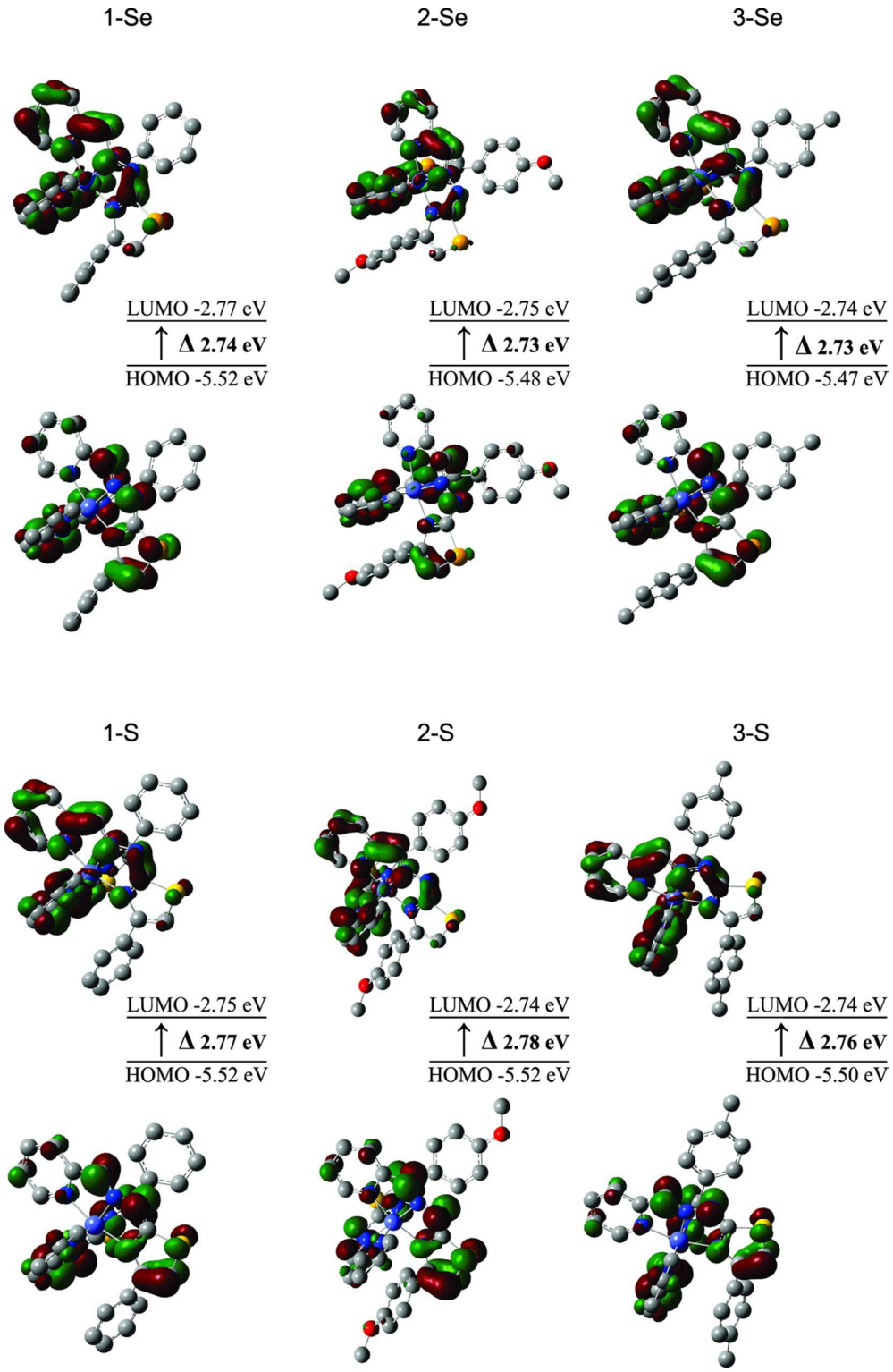

Fig. 6 Graphic representation of calculated HOMO, LUMO and HOMO-LUMO transition of Co(III) complexes with E-1,3-thiazoles and E-1,3-selenazoles as ligands, in DMF solvent.

DOI: 10.1039/C6DT04785H

Table 7 Antibacterial activity of investigated compounds tested by the disc-diffusion method.

	Inhibition zone diameter[a] (mm)							
Compound	*P. hauseri*	*P. aeruginosa*	*E. coli*	*S. enterica*	*S. aureus*	*C. sporogenes*	*B. subtilis*	*K. rhizophila*
HLSe[1]	10	10	10	10	10	10	10	10
HLSe[2]	10	10	12	14	12	12	12	14
HLSe[3]	10	12	12	12	10	10	12	12
HLS[1]	n.a.[b]	n.a.	n.a.	n.a.	n.a.	n.a.	n.a.	n.a.
HLS[2]	n.a.	n.a.	n.a.	n.a.	n.a.	n.a.	n.a.	n.a.
HLS[3]	n.a.	n.a.	n.a.	n.a.	n.a.	n.a.	n.a.	n.a.
1-Se	24	24	26	24	26	24	24	28
2-Se	28	26	28	26	26	28	26	30
3-Se	26	24	28	26	26	26	24	28
1-S	22	20	30	28	20	24	26	30
2-S	26	24	32	24	24	24	26	32
3-S	32	34	32	28	32	30	30	32
Amikacin	22	20	38	22	28	20	20	22

[a] Including diameter of disc (8 mm); [b] n.a. – not active

Table 8 LC_{50} values of the *A. salina* cytotoxic activity and IC_{50} of the DPPH free-radical scavenging activity of investigated compounds

Compound	LC_{50} (μM) *A. salina*	IC_{50} (μM) DPPH assay	Compound	LC_{50} (μM) *A. salina*	IC_{50} (μM) DPPH assay
HLS[1]	60.64 ± 9.23	81.97 ± 7.66	**HLSe[1]**	94.73 ± 6.56	50.74 ± 7.85
HLS[2]	144.99 ± 11.23	298.60 ± 18.14	**HLSe[2]**	137.15 ± 13.10	125.28 ± 15.22
HLS[3]	70.62 ± 7.04	151.12 ± 13.59	**HLSe[3]**	120.14 ± 12.45	73.15 ± 8.18
1-S	35.49 ± 5.74	48.93 ± 6.81	**1-Se**	72.66 ± 7.32	18.86 ± 4.93
2-S	66.71 ± 10.11	146.51 ± 16.64	**2-Se**	62.92 ± 8.89	70.67 ± 9.54
3-S	42.21 ± 9.87	71.71 ± 5.37	**3-Se**	72.41 ± 9.63	42.33 ± 6.41
$K_2Cr_2O_7$	248.14 ± 16.85	n.t[a]	Ascorbic acid	n.t.	79.38 ± 8.52

[a] n.t. – not tested

Complexes were more toxic than corresponding ligands. The results of greater toxicity of complexes in comparison to the ligands are not surprising. Considering that complexes possess great antibacterial activity and the fact that *A. salina* nauplii live in symbiosis with certain types of bacteria,[66] toxicity of the complexes is probably reflected in the lysis of the cell wall of bacteria present in the digestive tract of nauplii.

Free-radical scavenging activity

Selenium and sulphur inorganic and organic compounds and proteins are well known by their antioxidant properties.[67–70] On the other hand, there is only one study of antioxidant capacity of (1,3-thiazol-2-yl)hydrazones[71] while to the best of our knowledge there is no such study published for (1,3-selenazol-2-yl)hydrazones. The proton donating ability of investigated compounds was assayed using a protocol for the determination of radical scavenging activity, the 2,2-diphenyl-1-picrylhydrazyl (DPPH) method.[72] IC_{50} values were calculated from the plotted graph of scavenging activity against the concentrations of the samples. IC_{50} is defined as the total antioxidant necessary to decrease the initial DPPH radical by 50%. IC_{50} was calculated for all compounds based on the percentage of DPPH radicals scavenged. Ascorbic acid was used as the reference compound (positive control) with concentrations from 50 to 500 μg mL^{-1}. The obtained results (Table 8) revealed that selenium compounds were better antioxidants in comparison to their sulphur isosters, without exception. Both selenium and sulphur ligands with unsubstituted benzene rings showed best antioxidant activity in corresponding series. Benzene ring substitution with both electron donation (Me) and electron withdrawing properties (OMe) resulted in less active compounds. This effect was more

View Article Online
DOI: 10.1039/C6DT04785H

pronounced for OMe derivatives. The Co(III) complexes followed the same trend. It is interesting to notice that there is a total overlap between free-radical scavenging activity and cytotoxicity. Namely, the compounds showing the more pronounced free-radical scavenging activity were the most cytotoxic.

Co(III) complexes showed better activities than the corresponding ligands. Our results are challenging the previously postulated hypothesis regarding the mode of action of (1,3-thiazol-2-yl)hydrazones[70] and other hydrazono derivatives,[72] which indicate an interaction of hydrazone hydrogen atom with DPPH radical. Namely, the coordination of **HLS$^{(1–3)}$** to Co(III) resulted in their deprotonation, which was shown by the results of single crystal X-ray diffraction experiments. On the other hand there is no other acidic hydrogen atom present in Co complexes. It seems that sulphur and selenium atoms are the cause for free-radical scavenging activity in Co(III) complexes.

Conclusions

(1,3-Selenazol-2-yl)hydrazones **HLSe$^{(1–3)}$** were obtained by reaction of corresponding bromoacetophenones and 2-formylpyridine selenosemicarbazone in water/EtOH mixture. The choice of solvent leads to precipitation of *E* isomers and formation of a non-protonated species. The metal complexes with (1,3-selenazol-2-yl)hydrazones as ligands were prepared for the first time. Results of XRD confirmed bonding of pyridine and imine nitrogen atoms, which is a well known coordination behaviour of pyridyl-based hydrazone ligands. 1,3-Selenoazole ring contains two donor atoms capable of coordinating to Co(III) ions forming a chelate ring. XRD revealed a coordination of hard nitrogen atom instead of soft selenium atom to metal centre making (1,3-selenazol-2-yl)hydrazones NNN tridentate chelators.

UV-Vis spectral characterization in DMF was supported by TD-DFT calculations. Values of λ_{max} for selenoazole derivatives are shifted bathochromically. Calculated values of E_{gap} for selenoazoles are smaller than for their sulphur analogues which correlates to bathochromic shifts of λ_{max} for selenoazole derivatives. Energetically the most favourable ligand absorptions originate from HOMO→LUMO transitions. The HOMOs orbitals of all ligands and complexes are delocalized mainly at the azomethine group and selen/thiazole ring. These orbitals are also found at the benzene ring of the ligands and on Co atoms in the complexes. LUMOs of the ligands are delocalized on pyridine ring, azomethine group and selen/thiazole ring. Methyl- and methoxy- substituents of benzene ring destabilizes HOMO and LUMO orbitals and decreases the energy gap due to electron releasing effect. The LUMO orbitals of (**1–3**)-**Se** and (**1–3**)-**S** are delocalized mainly at the azomethine group, metal centre, and pyridine ring.

Electrochemical study of investigated sulphur and selenium ligands, supported by calculation of Fukui functions, indicate one-electron reduction process of C=N hydrazono group and one two-electron oxidation of C8-chalcogen bond. Totally, four-electron oxidations observed in the case of all complexes indicate that C8-chalcogen bond is a possible oxidation site, while only two reversible reduction processes observed were attributed to Co(III)→Co(II) and Co(II)→Co(I) reductions. Further possible reduction sites (Co(I) and C=N) are supposed to be at even lower potentials, outside the potential window applied in our CV experiments.

The investigation of free-radical scavenging activity of all substances indicates that selenium based compounds are more potent than corresponding sulphur analogues. The strong influence of substituents on benzene ring on free-radical scavenging activity was observed. Non-substituted derivatives appeared to be the most active ones in the case of all ligands and their complexes. **HLSe^2** and **HLS^2** were the only investigated compounds less active than the reference compound vitamin C.

Antimicrobial activity assay indicates that **HLSe$^{(1–3)}$** were more active than corresponding sulphur compounds on all bacterial and fungi strains investigated. Preparation of Co(III) complexes enhanced ligands' antibacterial activity. Despite the fact that sulphur based complexes reached almost the same level of antibacterial activity as their selenium analogues, results of acute lethality assay indicate the significantly smaller cell toxicity of Co(III) (1,3-selenazol-2-yl)hydrazone complexes, which makes them promising candidates for future antibacterial drug development.

Acknowledgements

The Ministry of Education, Science and Technological Development of the Republic of Serbia under Grant 172055 supported this work. S.G. acknowledges the COST CMST-Action CM1405 Molecules in Motion.

References

1 A. Borges, C. Ferreira, M. J. Saavedra and M. Simões, *Microb. Drug Resist.*, 2013, **19**, 256–265.
2 A. Ayati, S. Emami, A. Asadipour, A. Shafiee and A. Foroumadi, *Eur. J. Med. Chem.*, 2015, **97**, 699–718.
3 A. Z. Al-Rubaie, S. A. S. Al-Jadaan, S. K. Muslim, E. A. Saeed, E. T. Ali, A. K. J. Al-Hasani, H. N. K. Al-Salman and S. A. M. Al-Fadal, *J. Organomet. Chem.*, 2014, **774**, 43–47.
4 I. E. El-Shamy, A. M. Abdel-Mohsen, M. M. Al-Shehri, M. A. El-Hashashand and K. M. Al-Shamrani, *Life Sci. J.*, 2014, **11**, 385–391.
5 V. Zaharia, A. Ignat, B. Ngameni, V. Kuete, M. L. Moungang, C. N. Fokunang, M. Vasilescu, N. Palibroda, C. Cristea, L. Silaghi-Dumitrescu and B. T. Ngadjui, *Med. Chem. Res.*, 2013, **22**, 5670–5679.
6 G. F. Combs, Jr., *Nutrients*, 2015, **7**, 2209–2236.
7 L. D. Koller and J. H. Exon, *Can. J. Vet. Res.*, 1986, **50**, 297–306.
8 H. J. Reich and R. J. Hondal, *ACS Chem. Biol.*, 2016, **11**, 821–841.
9 K. C. Agrawal, B. A. Booth, R. L. Michaud, E. C. Moore and A. C. Sartorelli, *Biochem. Pharmacol.*, 1974, **23**, 2421–2429.
10 D. L. Klayman, J. P. Scovill, C. J. Mason, J. F. Bartosevich, J. Bruce and A. J. Lin, *Arzneimittelforschung.*, 1983, **33**, 909–12.
11 Z. Al-Eisawi, C. Stefani, P. J. Jansson, A. Arvind, P. C. Sharpe, M. T. Basha, G. M. Iskander, N. Kumar, Z. Kovacevic, D. J. R.

DOI: 10.1039/C6DT04785H

Lane, S. Sahni, P. V Bernhardt, D. R. Richardson and D. S. Kalinowski, *J. Med. Chem.*, 2016, **59**, 294–312.
12 V. Calcatierra, Ó. López, J. G. Fernández-Bolaños, G. B. Plata and J. M. Padrón, *Eur. J. Med. Chem.*, 2015, **94**, 63–72.
13 C. R. Kowol, R. Eichinger, M. A. Jakupec, M. Galanski, V. B. Arion and B. K. Keppler, *J. Inorg. Biochem.*, 2007, **101**, 1946–1957.
14 A. Molter, J. Rust, C. W. Lehmann, G. Deepa, P. Chiba and F. Mohr, *Dalt. Trans.*, 2011, **40**, 9810.
15 D. L. Klayman, J. P. Scovill, J. F. Bartosevich and J. Bruce, *J. Med. Chem.*, 1983, **26**, 35–39.
16 S. R. Turk, C. Shipman and J. C. Drach, *J. Gen. Virol.*, 1986, **67**, 1625–1632.
17 C. Pizzo, P. Faral-Tello, G. Salinas, M. Fló, C. Robello, P. Wipf and S. Graciela Mahler, *Medchemcomm*, 2012, **3**, 362.
18 H. G. Mautner, W. D. Kumler, Y. Okano and R. Pratt, *Antibiot. Chemother. (Washington, D. C.)*, 1956, **6**, 51–5.
19 M. D. Revenko, V. I. Prisacari, A. V Dizdari, E. F. Stratulat, I. D. Corja and L. M. Proca, *Pharm. Chem. J.*, 2011, **45**, 351–354.
20 H. Elshaflu, S. Bjelogrlić, C. D. Muller, T. R. Todorović, M. Rodić, A. Marinković and N. R. Filipović, *J. Coord. Chem.*, 2016, **69**, 3354–3366.
21 A. O. Abdelhamid, A. A. Fahmi and A. A. M. Alsheflo, 2013, **1**, 568–586.
22 F. Chimenti, B. Bizzarri, A. Bolasco, D. Secci, P. Chimenti, A. Granese, S. Carradori, M. D'Ascenzio, D. Lilli and D. Rivanera, *Eur. J. Med. Chem.*, 2011, **46**, 378–382.
23 F. Chimenti, S. Carradori, D. Secci, A. Bolasco, P. Chimenti, A. Granese and B. Bizzarri, *J. Heterocycl. Chem.*, 2009, **46**, 575–578.
24 N. R. Filipović, S. Bjelogrlić, A. Marinković, T. Ž. Verbić, I. N. Cvijetić, M. Senćanski, M. Rodić, M. Vujčić, D. Sladić, Z. Striković, T. R. Todorović and C. D. Muller, *RSC Adv.*, 2015, **5**, 95191–95211.
25 N. Graf and S. J. Lippard, *Adv. Drug Deliv. Rev.*, 2012, **64**, 993–1004.
26 T. W. Hambley, *Science (80-.).*, 2007, **318**, 1392–1393.
27 C. R. Munteanu and K. Suntharalingam, *Dalt. Trans.*, 2015, **44**, 13796–13808.
28 E. L. Chang, C. Simmers and D. A. Knight, *Pharmaceuticals*, 2010, **3**, 1711–1728.
29 L. M. T. Frija, A. J. L. Pombeiro and M. N. Kopylovich, *Coord. Chem. Rev.*, 2016, **308**, 32–55.
30 M. V. de O. Cardoso, L. R. P. de Siqueira, E. B. da Silva, L. B. Costa, M. Z. Hernandes, M. M. Rabello, R. S. Ferreira, L. F. da Cruz, D. R. Magalhães Moreira, V. R. A. Pereira, M. C. A. B. de Castro, P. V. Bernhardt and A. C. L. Leite, *Eur. J. Med. Chem.*, 2014, **86**, 48–59.
31 N. Filipović, T. Todorović, R. Marković, A. Marinković, S. Tufegdžić, D. Godjevac, K. Andjelković, *Transition Met. Chem.*, 2010, **35**, 765–772.
32 C. R. Kowol, W. Miklos, S. Pfaff, S. Hager, S. Kallus, K. Pelivan, M. Kubanik, É. A. Enyedy, W. Berger, P. Heffeter, B. K. Keppler, *J. Med. Chem.*, 2016, **59**, 6739−6752.
33 T. Pilati and A. Forni, *J. Appl. Crystallogr.*, 1998, **31**, 503–504.
34 T. Pilati and A. Forni, *J. Appl. Crystallogr.*, 2000, **33**, 417–417.
35 H. Zabrodsky, S. Peleg and D. Avnir, *J. Am. Chem. Soc.*, 1993, **115**, 8278–8289.
36 M. V. Rodić, V. M. Leovac, L. S. Jovanović, V. Spasojević, M. D. Joksović, T. Stanojković, I. Z. Matić, L. S. Vojinović-Ješić and V. Marković, *Eur. J. Med. Chem.*, 2016, **115**, 75–81.
37 M. Alagesan, N. S. P. Bhuvanesh and N. Dharmaraj, *Dalt. Trans.*, 2013, **42**, 7210.
38 V. M. Leovac, V. I. Češljević, L. S. Vojinović-Ješić, V. Divjaković, L. S. Jovanović, K. M. Szécsényi and M. V. Rodić, *Polyhedron*, 2009, **28**, 3570–3576.
39 M.-H. Shih, Y.-S. Su and C.-L. Wu, *Chem. Pharm. Bull. (Tokyo).*, 2007, **55**, 1126–1135.
40 C. Kleeberg and M. Bröring, *Polyhedron*, 2010, **29**, 507–513.
41 E. Ruiz, X. Tang, Y.-J. Li and M. M. Muir, *J. Crystallogr. Spectrosc. Res.*, 1993, **23**, 791–794.
42 Y. Qin, P. Shi, Q.-Y. Guan, X. Shi, G.-L. Zhao and W. H. Xuebao, *Chinese J. Inorg. Chem.*, 2013, **29**, 2013.
43 B.-B. Xu, P. Shi, Q.-Y. Guan, X. Shi and G.-L. Zhao, *J. Coord. Chem.*, 2013, **66**, 2605–2614.
44 T. V. Troepol'skaya and G. K. Budnikov, *Elektrokhimiya azometinov*, Nauka, Moscow, 1989.
45 R. S. Nicholson, *Anal. Chem.*, 1965, **37**, 1351–1355.
46 P. Zanello, *Inorganic electrochemistry: theory, practice and applications*, Royal Society of Chemistry, 2003.
47 L. Bjelica and L. Jovanović, *J. Electroanal. Chem. Interfacial Electrochem.*, 1986, **213**, 85–110.
48 C. R. Kowol, E. Reisner, I. Chiorescu, V. B. Arion, M. Galanski, D. V. Deubel and B. K. Keppler, *Inorg. Chem.*, 2008, **47**, 11032–11047.
49 D. Tomco, F. R. Xavier, M. M. Allard and C. N. Verani, *Inorg. Chim. Acta*, 2012, **393**, 269–275.
50 M. van der Meer, Y. Rechkemmer, U. Frank, F. D. Breitgoff, S. Hohloch, C.-Y. Su, P. Neugebauer, R. Marx, M. Dörfel, J. van Slageren and B. Sarkar, *Chem. Eur. J.*, 2016, **22**, 13884–13893.
51 I. Yilmaz, H. Temel and H. Alp, *Polyhedron*, 2008, **27**, 125–132.
52 T. Murai, K. Yamaguchi, F. Hori and T. Maruyama, *J. Org. Chem.*, 2014, **79**, 4930–4939.
53 N. Günay, E. Tarcan, D. Avcı, H. Cömert, K. Esmer and Y. Atalay, *Concepts Magn. Reson. Part A*, 2009, **34A**, 297–304.
54 H. Tavakol, *Struct. Chem.*, 2011, **22**, 1165–1177.
55 H. Hirao, *J. Phys. Chem. A*, 2011, **115**, 9308–9313.
56 J. N. Miller and J. C. Miller, *Statistics and Chemometrics for Analytical Chemistry*, Pearson Education Limited, England, 5th ed., 2005.
57 S. E. H. Etaiw, D. M. Abd El-Aziz, E. H. Abd El-Zaher and E. A. Ali, *Spectrochim. Acta Part A Mol. Biomol. Spectrosc.*, 2011, **79**, 1331–1337.
58 H. N. Ly, D. J. R. Brook and O. Oliverio, *Inorganica Chim. Acta*, 2011, **378**, 115–120.
59 S. Mukherjee, S. Chowdhury, A. P. Chattopadhyay and H. Stoeckli-Evans, *Polyhedron*, 2010, **29**, 1182–1188.
60 D. Sek, M. Siwy, K. Bijak, M. Grucela-Zajac, G. Malecki, K. Smolarek, L. Bujak, S. Mackowski and E. Schab-Balcerzak, *J. Phys. Chem. A*, 2013, **117**, 10320–10332.
61 J. V. Metzger, *The Chemistry of Heterocyclic Compounds, Thiazole and Its Derivatives*, John Wiley & Sons, Inc., United States, 2009.
62 L. A. Berben and J. R. Long, *Inorg. Chem.*, 2005, **44**, 8459–8468.
63 A. B. P. Lever, *Inorganic electronic spectroscopy*, Amsterdam, 1968.
64 P. F. Rapheal, E. Manoj, M. R. P. Kurup and E. Suresh, *Polyhedron*, 2007, **26**, 607–616.
65 G. Zhang and C. B. Musgrave, *J. Phys. Chem. A*, 2007, **111**, 1554–1561.
66 S. A. Soto-Rodriguez, N. Simões, D. A. Jones, A. Roque and B. Gomez-Gil, *J. Microbiol. Methods*, 2003, **52**, 101–14.
67 C. M. Weekley and H. H. Harris, *Chem. Soc. Rev.*, 2013, **42**, 8870.

View Article Online
DOI: 10.1039/C6DT04785H

68 E. Mukwevho, Z. Ferreira and A. Ayeleso, *Molecules*, 2014, **19**, 19376–19389.
69 R. R. Ramoutar and J. L. Brumaghim, *Cell Biochem. Biophys.*, 2010, **58**, 1–23.
70 M. Iwaoka and K. Arai, *Curr. Chem. Biol.*, 2013, **7**, 2–24.
71 M.-H. Shih, Y.-S. Su and C.-L. Wu, *Chem. Pharm. Bull. (Tokyo).*, 2007, **55**, 1126–1135.
72 R. L. Prior, X. Wu and K. Schaich, *J. Agric. Food Chem.*, 2005, **53**, 4290–4302.

View Article Online
DOI: 10.1039/C6DT04785H

Table of Contents Entry

Co(III) Complexes of (1,3-Selen-2-yl)hydrazones and Their Sulphur Analogues: Comparative Structural, Electrochemical, Computational and Biological Activity Study

Nenad R. Filipović[a], Hana Elshaflu[b], Sonja Grubišić[c], Ljiljana S. Jovanović[d], Marko Rodić[d], Irena Novaković[c], Aleksandar Marinković[e], Ivana S. Djordjević[c], Haidong Li[f], Nešo Šojić[f], Aleksandar Marinković[b], Tamara R. Todorović[e,*]

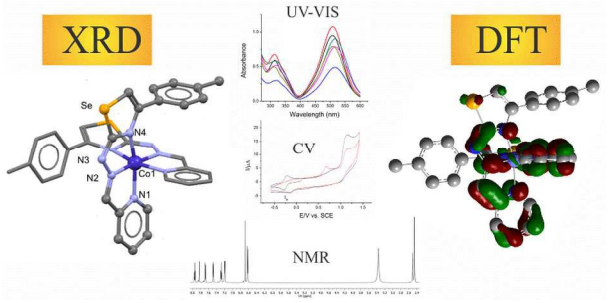

The first complexes of (1,3-selen-2-yl)hydrazones showed potent antibacterial and antioxidant activity and lower toxicity in comparison to their sulphur analogues.